

## Finite temperature strong-coupling expansions for the Kondo lattice model

J. Oitmaa and Weihong Zheng<sup>y</sup>

School of Physics, The University of New South Wales, Sydney, NSW 2052, Australia.

(Dated: April 14, 2024)

Strong-coupling expansions, to order  $(t/J)^8$ , are derived for the Kondo lattice model of strongly correlated electrons, in 1-, 2- and 3-dimensions at arbitrary temperature. Results are presented for the specific heat, and spin and charge susceptibilities.

## I. INTRODUCTION

This paper, the second of a sequence, studies the thermodynamic properties of the Kondo lattice model, described by the Hamiltonian

$$H = t \sum_{\langle ij \rangle} (c_i^\dagger c_j + \text{h.c.}) + J \sum_i S_i \cdot \sum_i n_i \quad (1)$$

The first term describes a single band of conduction electrons, the "Kondo coupling" term represents an exchange interaction between conduction electrons and a set of localized  $S = \frac{1}{2}$  spins, and the final term allows for variable conduction electron density via a chemical potential.

The Kondo lattice model combines two competing physical effects. In the strong coupling (large  $|J|$ ) limit, the conduction electrons will form local singlets ( $J > 0$ ) or triplets ( $J < 0$ ) with the localized spin at each site. In either case there will be a gap to spin excitations and spin correlations will be short ranged. On the other hand, at weak coupling, the conduction electrons can induce the usual RKKY interaction between localized spins, leading to magnetic order.

Despite the apparent simplicity of the model, no exact results are known, either at  $T = 0$  or at finite temperatures, in any spatial dimension. In the preceding paper<sup>1</sup> we studied the ground state properties of the model at  $T = 0$ , using linked-cluster series expansions. We refer to that paper for a discussion of other work, which has been, almost exclusively, restricted also to  $T = 0$ . In the present paper we focus on finite temperature thermodynamic properties. We know of only a few previous studies of this kind. Roder et al.<sup>2</sup> considered the ferromagnetic model in the limit  $J \rightarrow \infty$ , on the simple cubic lattice, via a high temperature expansion. Here we treat the general  $J$  case and focus on the antiferromagnetic model. Shibata et al.<sup>3</sup> have studied the 1D antiferromagnetic model via a finite-temperature DMRG approach. Haule et al.<sup>4</sup> have treated the 2D case, primarily via a numerical finite temperature Lanczos method. We compare our results with this work wherever possible. Haule et al. have also considered the atomic limit ( $t = 0$ ), and the order  $t^2$  correction terms. Our work was largely motivated by this paper.

Our approach, which will be described in the following Section, treats the single site terms exactly and treats the hopping term perturbatively. It is, thus, an expansion about the "atomic limit". We summarize here, for completeness and for later reference, the exact results in this limit.

For variable conduction electron density there are 8 states per site: 2 states with no conduction electrons and localized spin up or down, 2 states with two conduction electrons of opposite spin, and 4 states (a singlet and 3 triplets) with one conduction electron coupled to the localized spin. For a lattice of  $N$  sites the grand partition function is

$$Z_0 = \text{Tr} e^{-\beta H_0} = Z_0^N \quad (2)$$

with

$$z_0 = 2 + (e^{3K} + 3e^K) + 2^2 \quad (3)$$

and  $K = J/4$ ,  $\mu = e$ ,  $\beta = 1/k_B T$ .

The internal energy per site is given by

$$\begin{aligned} u(\mu; T) &= \frac{\partial}{\partial \beta} \ln z_0 \\ &= \frac{\frac{3}{4}J(e^{3K} + 3e^K)}{2 + (e^{3K} + 3e^K) + 2^2} \end{aligned} \quad (4)$$

The fugacity can, as usual, be eliminated in favour of the electron density  $n$  by using the relation

$$\begin{aligned} n(\mu; T) &= \frac{\partial}{\partial \mu} \ln z_0 \\ &= \frac{q + 2^2}{1 + q + 2^2} \end{aligned} \quad (5)$$

where we have introduced  $q = \frac{1}{2}(e^{3K} + 3e^K)$ . Solving this gives

$$= \frac{q(1-n) + \frac{1}{2}q^2(1-n)^2 + 4n(2-n)}{2(2-n)} \quad (6)$$

The specific heat is then obtained from (4) and (6) via the usual relation  $C_v = \frac{du}{dT}$ .

Also of interest are the compressibility or "charge susceptibility"

$$\chi_c = \frac{\partial n}{\partial \mu} \quad (7)$$

which can be expressed as

$$\chi_c = \frac{q(1-n) + 2(2-n)^2}{1 + q + 2^2} \quad (8)$$

and the magnetic susceptibility, which is given by

$$\chi_s = \frac{1 + 4e^K + 2^2}{1 + q + 2^2} \quad (9)$$

Simpler analytic results can be obtained in various limits: at high or low temperature, and at or near half-filling. Some of these are given in Ref. 4, although they contain minor errors in a few cases.

Of course in the atomic limit all of these quantities are smooth functions of temperature and electron density.

## II. THERMODYNAMIC PERTURBATION THEORY

Our goal is to obtain an expression for the thermodynamic potential, and hence other quantities, in powers of  $t=J$ . We work in the grand canonical ensemble and write the Hamiltonian as

$$H = H_0 + V \quad (10)$$

with

$$H_0 = J \sum_i S_i \cdot S_i + \sum_i \epsilon_i n_i \quad (11)$$

$$V = \sum_{\langle ij \rangle} t_{ij} (c_i^\dagger c_j + \text{h.c.}) \quad (12)$$

The grand partition function can then be expanded in the usual way as

$$\begin{aligned} Z_g &= \text{Tr} e^{-(H_0 + V)} g \\ &= Z_0 \left[ 1 + \sum_{r=1}^{\infty} \frac{(-1)^r}{r!} \text{Tr} \left( \frac{V}{Z_0} \right)^r \right] \end{aligned} \quad (13)$$

with

$$V = e^{H_0} V e^{-H_0} \quad (14)$$

and

$$\langle H \rangle = \frac{1}{Z_0} \text{Tr} e^{-H_0} H g \quad (15)$$

where  $Z_0$  is the atomic limit partition function (2). The free energy (grand potential) is then given by

$$F = N \ln Z_0 + \sum_{r=1}^{\infty} \frac{(-1)^r}{r!} \text{Tr} T_r \quad (16)$$

where

$$T_r = \frac{1}{Z_0} \text{Tr} \left( \frac{V}{Z_0} \right)^r g \quad (17)$$

and the subscript  $N$  signifies that only the part proportional to  $N$  is to be included.

This approach is, of course, well known and has been used in the past for both pure spin models<sup>5</sup> and for the Hubbard model<sup>6</sup>. Any contribution to  $T_r$  in (17) comes from a particular cluster of sites and bonds, a "graph". It is possible to restrict the class of graphs to connected ones only, as done in Ref. 5. In our work we included also disconnected graphs, of more than one component, as they are rather easy to deal with directly. Since each bond contributes a  $V$  operator and hence a factor  $t$ , it is obvious that to carry the expansion to order  $t^r$  all topologically distinct graphs with up to  $r$  bonds need to be considered. There are a total of 115 graphs through 8th order, which is as far as we have been able to compute.

The contribution of a particular graph  $G$  to the free energy can be expressed in the form

$$T_r(G) = C_G (t/J)^r Z_0^p \sum_{s;l;m} a_{s;l;m} K^l e^{mK} \quad (18)$$

where  $C_G$  is the embedding factor, or "weak lattice constant" of graph  $G$  in the particular lattice considered,  $p$  is the number of points or vertices in the graph, the  $a_{s;l;m}$  are numerical constants, and the sum contains, for each graph, a finite set of terms labeled by integers  $s;l;m$ . Evaluation of these expressions is a lengthy procedure, involving a trace over a space of  $8^p$  states and evaluation, for each term in the trace, of an  $r$ -fold multiple integral. It is possible to find many time saving remarks, but, even so, the evaluation of the worst case, the octagon, took some 260 hours of CPU time on a 1GHz Compaq alpha processor.

Having computed the  $T_r(G)$  factors for all graphs it is then a simple matter to combine these and to obtain, for any lattice, the free energy per site in the form

$$f = \ln Z_0 + \sum_{r=2}^{\infty} \frac{(-1)^r}{r!} F_r(K; t/J) \quad (19)$$

where the  $F_r$  are complete expressions in  $K$  and  $t/J$ , of the form

$$F_r(K; t/J) = \sum_{s;l;m} a_{s;l;m} K^l e^{mK} \quad (20)$$

These expressions are too lengthy to display here, but can be supplied on request. To give some idea of the size, the 8th order factor  $F_8$  contains 1042 separate terms.

From (19) and (20) one can compute expressions for the internal energy and specific heat. The internal energy can be expressed in the form

$$\begin{aligned} u &= \frac{\partial}{\partial \beta} (\ln f) \\ &= u_0 + \sum_{r=2}^{\infty} z_0^{(r+1)} E_r(K; \beta) (t=\beta)^r \end{aligned} \quad (21)$$

where  $u_0$  is the atomic limit result (4) and the  $E_r(K; \beta)$  are complete expressions. The specific heat is  $C_v = du/dT$ . For most purposes it is more useful to express the series in terms of electron density  $n$ , which can be obtained from (19) via

$$\begin{aligned} n &= \frac{\partial}{\partial \beta} (\ln f) \\ &= n_0 + \sum_{r=2}^{\infty} z_0^{(r+1)} Y_r(K; \beta) (t=\beta)^r \end{aligned} \quad (22)$$

where  $n_0$  is the atomic limit result (5) and the  $Y_r(K; \beta)$  are, again, complete expressions in  $K, \beta$ . For fixed  $n$  and  $K$  we then use a numerical reversion procedure to obtain expansions for the fugacity, in power of  $t=\beta$ , which can then be eliminated from the thermodynamic functions. For half-filling ( $n = 1$ ) this reversion can be carried out analytically.

In addition we have included a magnetic field term

$$H^0 = H - h \sum_i^X (n_{i,\uparrow} - n_{i,\downarrow} + 2S_i^z) \quad (23)$$

to allow calculation of the zero-field magnetic susceptibility  $\chi_s$ , which is expressed in the form

$$\chi_s = \chi_0 + \sum_{r=2}^{\infty} z_0^{(r+1)} X_r(K; \beta) (t=\beta)^r \quad (24)$$

where, again, the first term is the atomic limit result (9) and the  $X_r$  are complete expressions. The fugacity can again be eliminated in favour of the electron density, as described above.

Several checks on the correctness of our results have been made. Since temperature enters explicitly, we can take the zero temperature ( $K \rightarrow 1$ ) limit analytically, to recover the ground state energy series<sup>1,7</sup>. Another test is the  $\beta \rightarrow 0$  limit, in which  $F_r(K; \beta)$  in (19) has a leading term of order  $K^r$ , giving an expression in powers of  $(\beta)$ . This can be compared with the results for free electrons. Complete agreement is obtained. We are confident that our results are correct, but cannot exclude the possibility of errors not picked up by these checks.

The analysis of the results follows standard lines. For any fixed  $K; \beta$  we obtain expressions for thermodynamic quantities as a series in the single variable  $(t=\beta)$ . For small  $t=\beta$  the series converges rapidly and even a naive sum gives good accuracy. Padé approximants and integrated differential approximants<sup>9</sup> allow extrapolation to larger  $(t=\beta)$ . For fixed  $n$  we obtain series for  $\chi_s$  in terms of  $t=\beta$ , which are then substituted into corresponding expressions (20), (24) to obtain a single-variable series in  $(t=\beta)$ , which is then evaluated as before. To calculate the specific heat it is necessary to include derivatives of  $\chi_s$  with respect to temperature. For the benefit of the reader we give in Table I coefficients for some representative cases. Other series can be supplied on request.

While the general expressions are too lengthy to write down, at high temperatures, one can expand the various quantities in powers of  $\beta$  or  $K$ . The expressions up to order  $K^4$  are provided in the Appendix. These are valid for all bcc-packed/bipartite lattices.

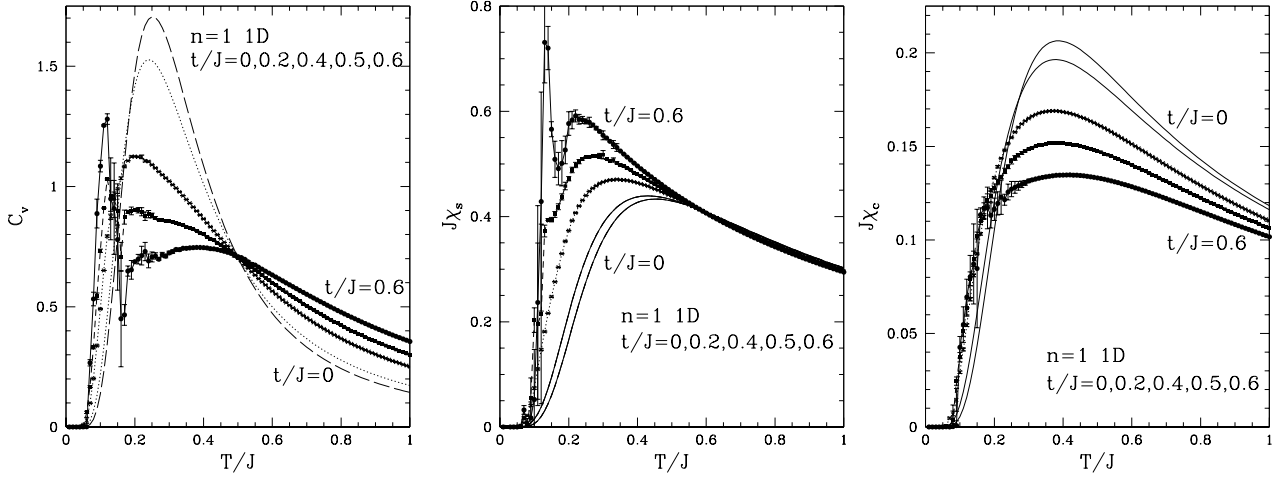


FIG. 1: The specific heat  $C_v$  (a), magnetic susceptibility  $\chi_s$  (b) and charge susceptibility  $\chi_c$  (c) versus  $T/J$  for the linear chain at  $n = 1$  for  $t/J = 0; 0.2; 0.4; 0.5; 0.6$ .

In the following sections we present results for the linear chain, the square lattice (sq) and the simple cubic (sc) lattice. A discussion of other lattices will be presented elsewhere.

### III. THE 1D KONDO LATTICE MODEL

We consider the antiferromagnetic model on a linear chain, with arbitrary electron concentration  $n$ . Using the procedure described above we have computed the specific heat and spin and charge susceptibilities. Figure 1 (a), (b) (c) shows these quantities, as functions of temperature, for  $n = 1$  (half-filling) for  $t/J = 0; 0.2; 0.4; 0.5; 0.6$ . For  $t/J < 0.4$  the series are well converged and the curves are obtained simply from the partial sums. For the larger values integrated differential approximants have been used, with the error bars indicating the variation between different approximants. Good agreement is obtained with the DMRG results for all three quantities. However our (relatively short) series are unable to probe the larger  $t/J$  region as well as DMRG can.

Some comments on Fig. 1 are in order. Fig. 1 (a) shows the specific heat, which shows an interesting crossover from a single peak for small  $t$  to a two-peak structure at larger  $t$ . In the larger  $t$  region the high temperature peak

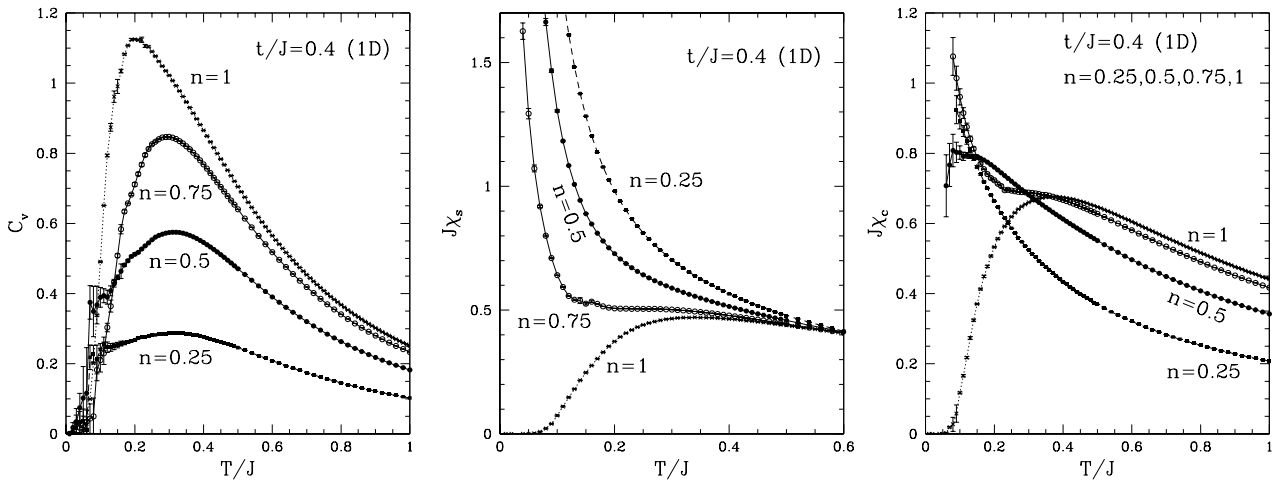


FIG. 2: The same as Fig. 1, but for  $t/J = 0.4$  and  $n = 1; 0.75; 0.5; 0.25$ .

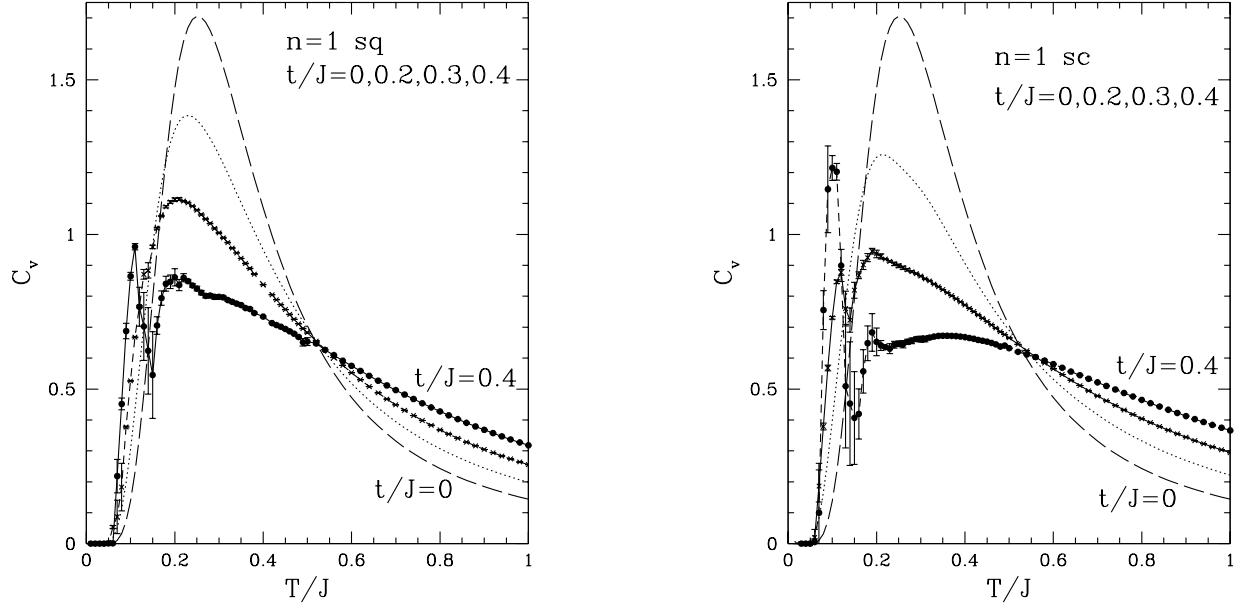


FIG. 3: The specific heat  $C_v$  versus  $T/J$  for square lattice (a) and simple cubic lattice (b) at  $n = 1$  for  $t/J = 0, 0.2, 0.3, 0.4$ .

becomes broadened and less prominent and is, presumably, due to conduction electrons whereas the low-temperature peak arises from the fluctuating local spins. The spin susceptibility (Fig. 1(b)) also has a peak at a characteristic temperature. The peak is enhanced and moves to lower  $T$  on increasing the hopping parameter  $t$ . Increasing  $t/J$  will weaken the singlet correlations and a lower characteristic temperature is sufficient for them all fluctuations to become dominant. There is some indication of a double peak for  $t/J = 0.6$ , but this may be an artifact of the numerical analysis. The charge susceptibility also has peak at a characteristic temperature, and a rapid drop to zero at low temperatures. The peak is depressed with increasing  $t$  but the position stays relatively constant.

To display the effect of varying conduction electron density we have chosen an intermediate value  $t/J = 0.3$  and show, in Fig. 2(a), (b), (c) curves of  $C_v$ ,  $\chi_s$  and  $\chi_c$  versus temperature for  $n = 1, 0.75, 0.5$  and  $0.25$ . The high-

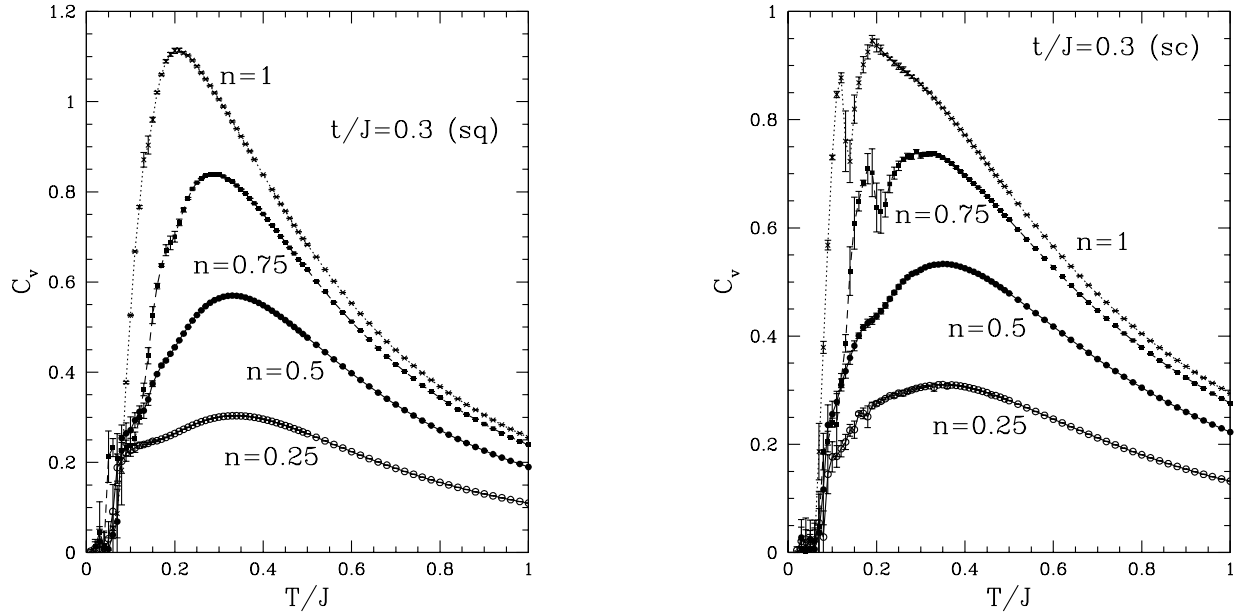


FIG. 4: The specific heat  $C_v$  versus  $T/J$  for square lattice (a) and simple cubic lattice (b) at  $t/J = 0.3$  for  $n = 1, 0.75, 0.5, 0.25$ .

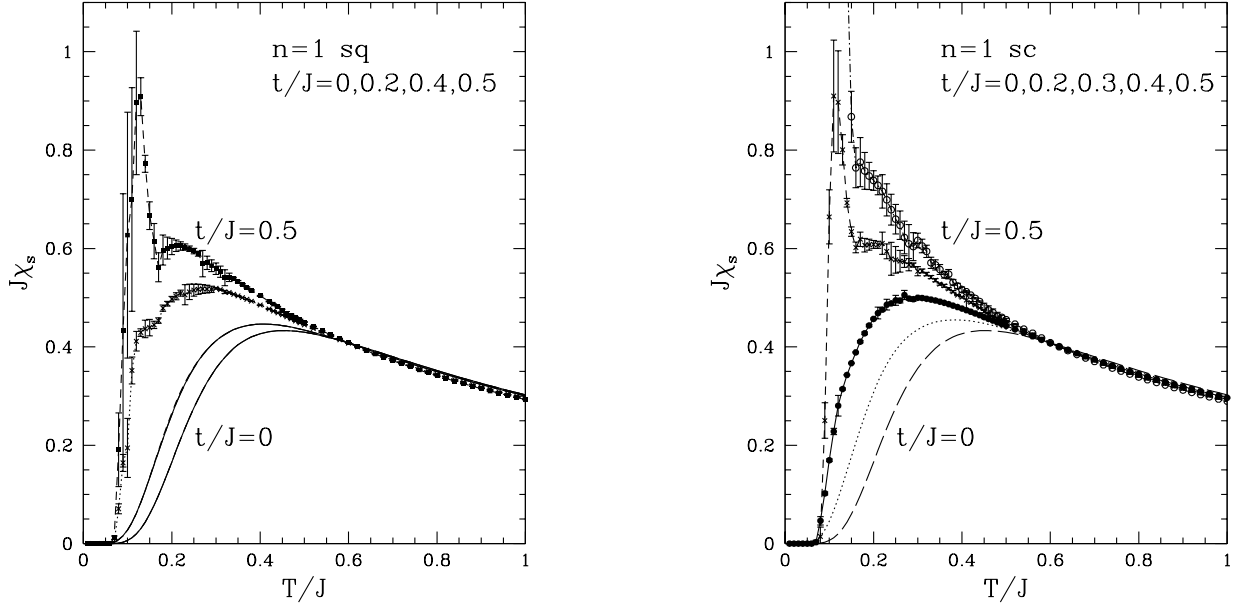


FIG. 5: The magnetic susceptibility  $\chi_s$  versus  $T/J$  for square lattice (a) and simple cubic lattice (b) at  $n = 1$  for  $t/J = 0; 0.2; 0.3; 0.4$ .

temperature peak in  $C_v$  (Fig. 2 (a)) drops roughly proportionally to  $n$ , in agreement with the assignment of this peak to conduction electrons. The series do not allow the low- $T$  specific heat to be determined with sufficient precision to see the effects of doping. Tsunetsugu et al.<sup>8</sup> present a ground state phase diagram of the 1D Kondo lattice (Fig. 6 of Ref. 8), where a transition line separates a small  $n$  ferromagnetic phase from a large  $n$  paramagnetic phase. For the parameter ratio  $t/J = 0.4$  the critical doping is  $n_c \approx 0.65$ . While there cannot be true order at finite temperature, the marked change in the low  $T$  specific heat between the two curves with  $n = 0.75$  and  $0.5$  may well be a reflection of this effect. The effect of doping on  $\chi_s$  is dramatic. For  $n = 1$ , at low temperatures, the system is in a gapped singlet phase and  $\chi_s$  goes to zero exponentially. Away from half-filling there will be free spins and  $\chi_s$  diverges according to the usual Curie law. The charge susceptibility  $\chi_c$  also shows a sharp crossover between the undoped and doped cases.

The 1D results are consistent with the, presumably, more accurate DMRG calculations. We are not aware of any published DMRG results for specific heat at finite doping, or for the susceptibility for  $n < 0.8$ . Our results confirm that the series approach can be successfully applied to this model. We now turn to the 2D and 3D cases, where far less is known and where other methods have particular difficulties.

#### IV. THE 2D AND 3D SYSTEMS

We have computed and analysed series for the specific heat, spin susceptibility and charge susceptibility for both the square and simple cubic lattices. Some representative series are given in Table I. We choose to present results for the two lattices together so as to highlight similarities and differences between them.

Figure 3 shows the specific heat at half-filling for various  $t/J$  ratios. The qualitative behaviour is similar to the 1D case, although smaller values of  $t/J$  suffice to produce comparable deviations from the atomic limit. A two-peak structure is manifest at  $t/J = 0.4$ . Figure 4 shows the dependence of the specific heat on doping (for fixed  $t/J = 0.3$ ). The decrease with decreasing  $n$  again confirms that the high  $T$  specific heat is due to conduction electrons. Figures 5 and 6 show the magnetic susceptibility, at half-filling for various  $t/J$  and at  $t/J = 0.3$  for various electron densities. Figure 6 shows a striking crossover from  $n = 1$ , where  $\chi_s$  is structureless and vanishes as  $T \rightarrow 0$  to lower densities

$n = 0.5$  and  $0.25$  where  $\chi_s$  appears to diverge. Evidently  $n = 0.75$  is near the critical concentration, as  $\chi_s$  appears to start to diverge but then drops to zero. There is also some apparent structure for the 3D case at  $T=J^{-1} \approx 0.15$ , which may be an artifact of the analysis.

A mean-field treatment<sup>8</sup> suggests the existence of a finite-temperature phase transition to a ferromagnetic phase for small  $n$ , at least for the 3D case. To explore this we plot the inverse susceptibility versus  $T$  in Figure 7. For both lattices  $\chi_s^{-1}$  appears to vanish linearly as  $T \rightarrow 0$  at  $n = 0.5$ . For the simple cubic lattice there is some indication that the curves for  $\chi_s^{-1}$  at  $n = 0.25$  and  $n = 0.1$  vanish at a small finite  $T$ , confirming a finite temperature ferromagnetic phase. However the analysis at low temperature is imprecise and does not allow for an accurate determination of  $T_c$ . The data for the square lattice appear to show no finite temperature ferromagnetic transition.

Finally in Figures 8 and 9 we show the charge susceptibility versus temperature. The behaviour is qualitatively similar to the 1D case.

## V. CONCLUSIONS

We have used thermodynamic perturbation theory to investigate the antiferromagnetic Kondo lattice model at finite temperatures. Our calculations focus, in particular, on the specific heat and spin and charge susceptibilities, and their variation both with the ratio  $t=J$  and with electron concentration. We have presented results for the linear chain, square lattice, and simple cubic lattice.

Overall, for the parameter region where our series can be analysed with reasonable precision, the behaviour of the 3 lattices is qualitatively similar. This is to be expected at moderate and high temperatures. We do, however, see an indication of a finite temperature ferromagnetic transition in 3-dimensions for small  $n$ , consistent with expectations. This is not seen in 1- and 2-dimensions.

For the linear chain our results are in excellent agreement with the previous finite-temperature DMRG calculations<sup>3</sup>, and serve to confirm the accuracy of both methods. There are few existing results in higher dimension and our work

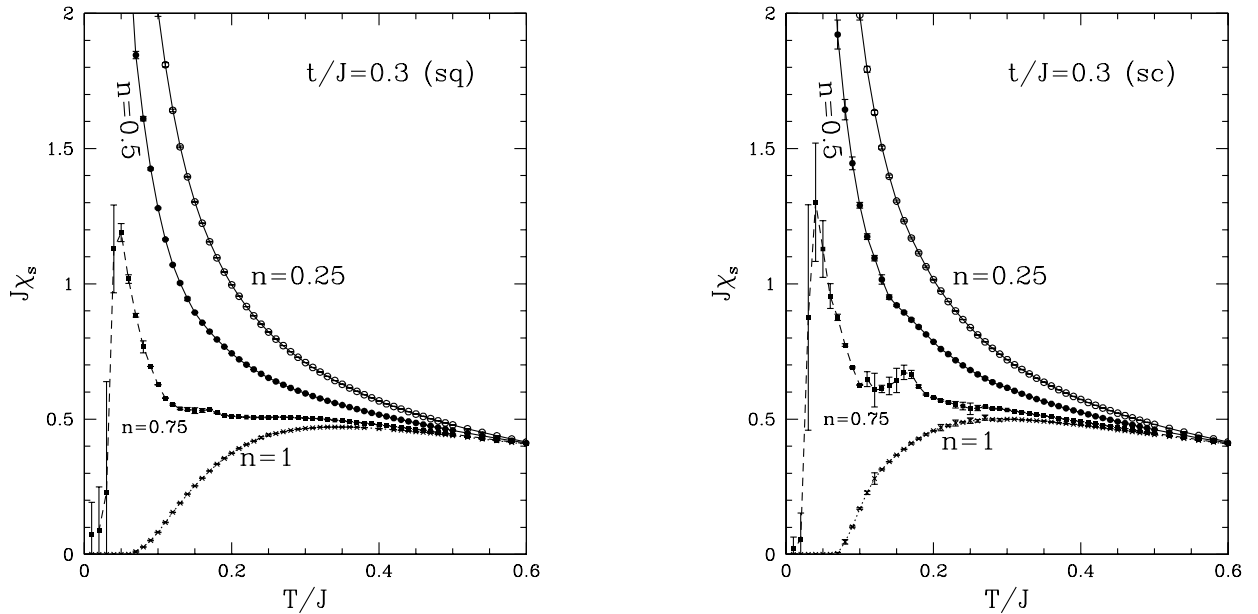


FIG. 6: The magnetic susceptibility  $\chi_s$  versus  $T=J$  for square lattice (a) and simple cubic lattice (b) at  $t=J = 0.3$  for  $n = 1; 0.75; 0.5; 0.25$ .



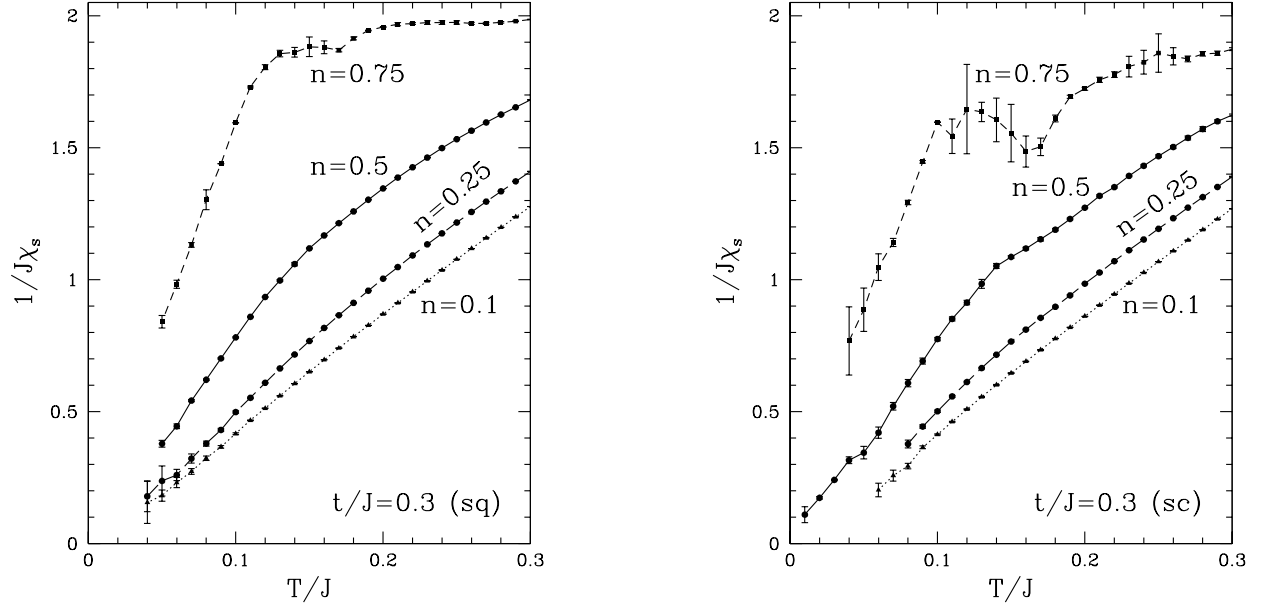


FIG. 7: The inverse of magnetic susceptibility  $1/\chi_s$  versus  $T/J$  for square lattice (a) and simple cubic lattice (b) at  $t/J = 0.3$  for  $n = 0.75; 0.5; 0.25; 0.1$ .

should provide a valuable benchmark for other approaches. While we have not attempted a detailed comparison on our  $t$  to experiment, this would be possible. We plan to report results for closed-packed lattices (triangular and face-centered cubic) and for the ferromagnetic Kondo lattice model elsewhere.

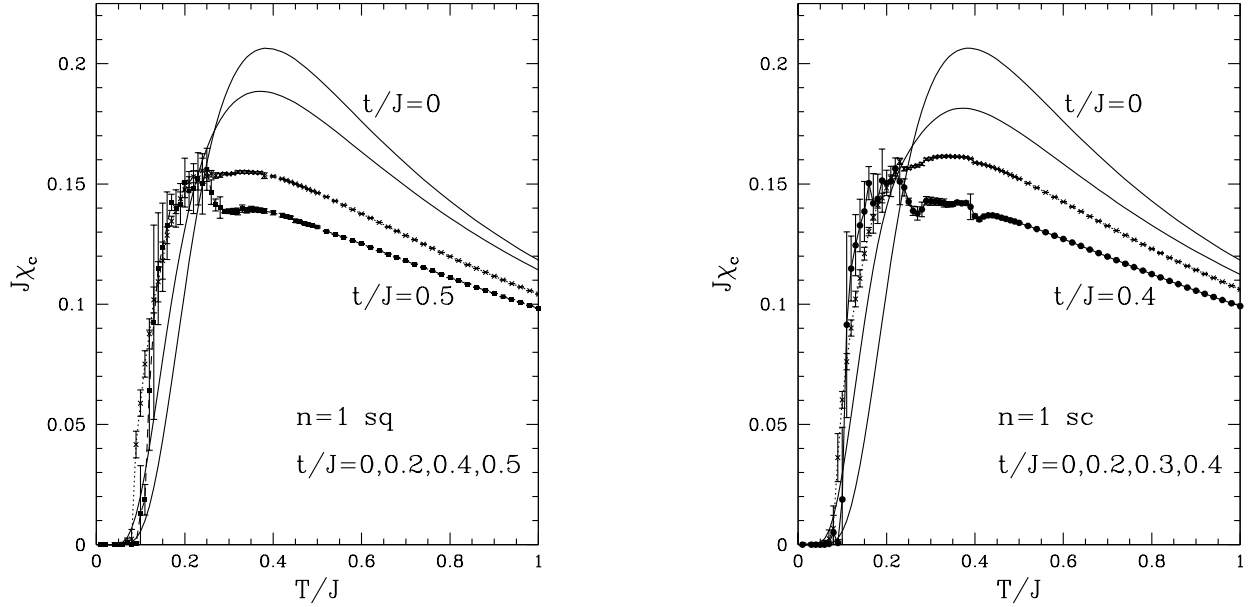


FIG. 8: The charge susceptibility  $\chi_c$  versus  $T/J$  for square lattice (a) and simple cubic lattice (b) at  $n = 1$  for  $t/J = 0; 0.2; 0.3; 0.4$ .

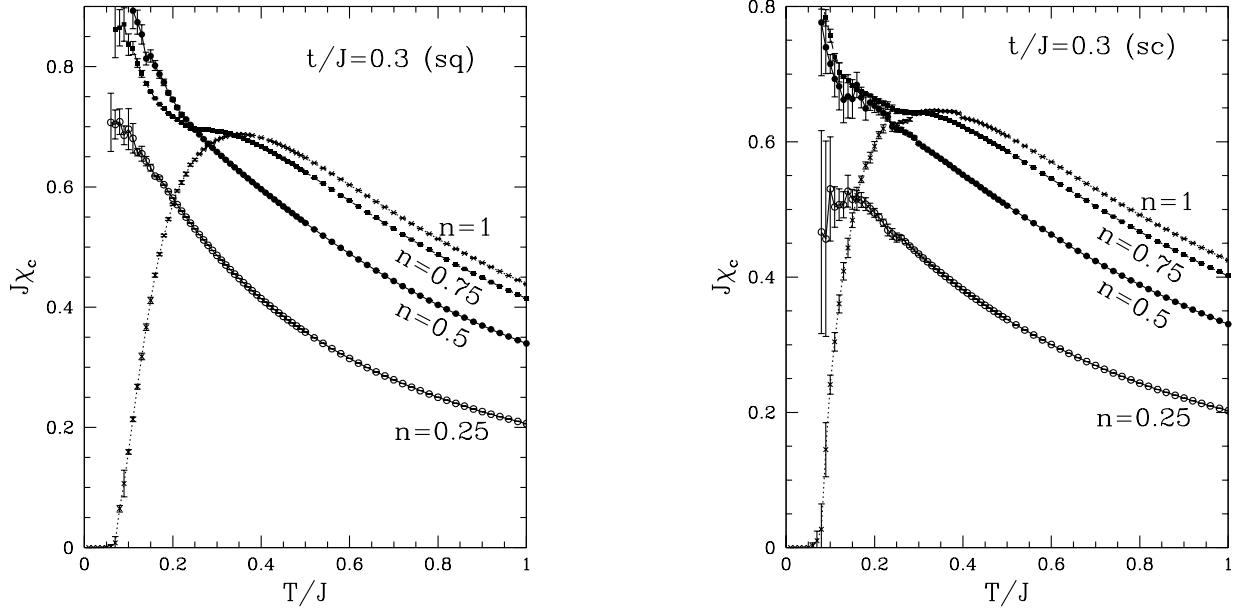


FIG. 9: The charge susceptibility  $\chi_c$  versus  $T/J$  for square lattice (a) and simple cubic lattice (b) at  $t/J = 0.3$  for  $n = 1; 0.75; 0.5; 0.25$ .

### Appendix

The following high temperature expansions up to order  $K^4$  have been obtained from the general results. The series are expressed in terms of  $K = J/4$ . The parameters are  $\beta = t/J$ ,  $z$  = coordination number,  $p_4$  is weak embedding constant of square cluster, which has value 0, 1, 3, and 12 for 1D, square lattice, simple cubic lattice, and BCC lattice, respectively, and  $z_2 = 2(4p_4 + z + z^2)/3$ .

Fugacity :

$$\begin{aligned} &= \frac{n}{2-n} - \frac{n(1-n)}{2-n} \left( \frac{3}{2} + 8z^2 \right) K^2 + K^3 \\ &\quad - \frac{1}{8} (11 - 27n + 9n^2) K^4 - 4z(4 - 3n) K^4 \\ &\quad - 32z(1 - 6n + 3n^2) K^4 - 32z_2(1 + n - n^2) K^4 + O(K^5) \end{aligned} \quad (25)$$

Internal energy:

$$\begin{aligned} u/J = & \frac{1}{32} n(2-n) \left( (12 + 64z^2)K + 12K^2 - (4 - 18n + 9n^2)K^3 - 64z^2K^3 \right. \\ & \left. - 256z(2 - 6n + 3n^2)K^3 - 256z_2n(2 - n)K^3 - 5(4 - 6n + 3n^2)K^4 - 80z^2K^4 + O(K^5) \right) \end{aligned} \quad (26)$$

Specific heat:

$$\begin{aligned} C_V/k_B = & n(2-n)K^2 \left( \frac{3}{2} + 8z^2 \right) + 3K \left( \frac{3}{8} (4 - 18n + 9n^2)K^2 - 24z^2K^2 \right. \\ & \left. - 96z(2 - 6n + 3n^2)K^2 - 96z_2n(2 - n)K^2 + O(K^5) \right) \end{aligned} \quad (27)$$

Magnetic susceptibility:

$$\begin{aligned} \chi_s = & \frac{1}{4} + \frac{1}{8} n(2-n) - 2K \left( \frac{1}{4} (8 - 6n + 3n^2)K^2 - 4zn(2 - n)K^2 \right. \\ & \left. + \frac{1}{3} (2 - 6n + 3n^2)K^3 + 8zn(2 - n)K^3 \right) \end{aligned}$$

$$\begin{aligned}
& + \frac{1}{24} (80 - 180n + 198n^2 - 108n^3 + 27n^4) K^4 + \frac{2}{3} z (12 + 10n - 41n^2 + 36n^3 - 9n^4) K^4 \\
& + 16zn (2 - n) (7 - 18n + 9n^2) K^4 - 32z_2 n (2 - n) (1 - 4n + 2n^2) K^4 + O(K^5)
\end{aligned} \tag{28}$$

Charge susceptibility:

$$\begin{aligned}
\chi_c = & \frac{1}{2} n (2 - n) - n^2 (2 - n)^2 \left( \frac{3}{8} + 2z^2 \right) K^2 + \frac{1}{4} K^3 \\
& - \frac{1}{16} (10 - 18n + 9n^2) K^4 - z (1 + 6n - 3n^2) K^4 \\
& - 8z (7 - 18n + 9n^2) K^4 + 16z_2 (1 - 4n + 2n^2) K^4 + O(K^5)
\end{aligned} \tag{29}$$

#### ACKNOWLEDGMENTS

This work forms part of a research project supported by a grant from the Australian Research Council. The computations were performed on an AlphaServer SC computer. We are grateful for the computing resources provided by the Australian Partnership for Advanced Computing (APAC) National Facility.

---

j.oitimaa@unsw.edu.au

<sup>y</sup> w.zheng@unsw.edu.au; <http://www.phys.unsw.edu.au/~zwh>

<sup>1</sup> W. H. Zheng and J. O. Tilmann, Phys. Rev. B (preceding paper).

<sup>2</sup> H. Roder, R. R. P. Singh and J. Zang, Phys. Rev. B 56, 5084 (1997).

<sup>3</sup> N. Shibata, B. Aumônier, M. Troyer, M. Sigrist and K. Ueda, J. Phys. Soc. Japan 67, 1086 (1998); N. Shibata and H. Tsunetsugu, ibid. 68, 744 (1999).

<sup>4</sup> K. Haule, J. Bonca, and P. P. Reddy, Phys. Rev. B 61, 2482 (2000).

<sup>5</sup> N. Elstner, and R. R. P. Singh, Phys. Rev. B 57, 7740 (1998).

<sup>6</sup> J. A. Henderson, J. O. Tilmann and M. C. B. Ashley, Phys. Rev. B 46, 6328 (1992).

<sup>7</sup> Z. P. Shi, R. R. P. Singh, M. P. Gelfand and Z. Wang, Phys. Rev. B 51, 15630 (1995).

<sup>8</sup> H. Tsunetsugu, M. Sigrist & K. Ueda, Rev. Mod. Phys. 69, 809 (1997).

<sup>9</sup> A. J. Guttmann, in "Phase Transitions and Critical Phenomena", Vol. 13 ed. C. Domb and J. Lebowitz (New York, Academic, 1989).

TABLE I: Series coefficients for the internal energy  $u$ , specific heat  $C_v$ , magnetic susceptibility  $\chi_s$  and charge magnetic susceptibility  $\chi_c$  at  $J = 1$  and electron densities  $n = 1; 0.5$  for the linear chain, the square lattice and the simple cubic lattice. Nonzero coefficients ( $t=J$ )<sup>r</sup> up to order  $r = 8$  are listed.

r	linear chain		square lattice		simple cubic lattice	
	n = 1	n = 0.5	n = 1	n = 0.5	n = 1	n = 0.5
$u=J$						
0	-1.18727275 $10^{-1}$	-8.78192521 $10^{-2}$	-1.18727275 $10^{-1}$	-8.78192521 $10^{-2}$	-1.18727275 $10^{-1}$	-8.78192521 $10^{-2}$
2	-9.19083667 $10^{-1}$	-6.90488388 $10^{-1}$	-1.83816733	-1.38097678	-2.75725100	-2.07146516
4	2.02166868 $10^{-1}$	1.94156599 $10^{-1}$	1.23945460	8.51133343 $10^{-1}$	3.11186319	1.97093023
6	-5.81316838 $10^{-2}$	-6.82352222 $10^{-2}$	-1.24540759	-8.52057857 $10^{-1}$	-5.90066730	-2.95078662
8	1.71426415 $10^{-2}$	2.25662666 $10^{-2}$	1.38876432	9.81227389 $10^{-1}$	1.32149047 $10^{-1}$	5.06962222
$C_v=k_B$						
0	1.44045799 $10^{-1}$	1.03910138 $10^{-1}$	1.44045799 $10^{-1}$	1.03910138 $10^{-1}$	1.44045799 $10^{-1}$	1.03910138 $10^{-1}$
2	7.42355042 $10^{-1}$	5.62969188 $10^{-1}$	1.48471008	1.12593838	2.22706513	1.68890757
4	-5.05380430 $10^{-1}$	-4.99348745 $10^{-1}$	-3.16863938	-2.18170564	-7.98977684	-5.04707069
6	2.39575311 $10^{-1}$	2.94484197 $10^{-1}$	5.37297355	3.70460027	2.57521720 $10^{-1}$	1.27479126 $10^{-1}$
8	-9.61839414 $10^{-2}$	-1.34812280 $10^{-1}$	-8.40726263	-6.02787617	-8.15089318 $10^{-1}$	-3.07784724 $10^{-1}$
$\chi_s$						
0	3.02552920 $10^{-1}$	2.88871928 $10^{-1}$	3.02552920 $10^{-1}$	2.88871928 $10^{-1}$	3.02552920 $10^{-1}$	2.88871928 $10^{-1}$
2	-2.69346503 $10^{-2}$	-1.34119052 $10^{-2}$	-5.38693006 $10^{-2}$	-2.68238104 $10^{-2}$	-8.08039510 $10^{-2}$	-4.02357157 $10^{-2}$
4	1.33858987 $10^{-2}$	7.41933727 $10^{-3}$	8.14693283 $10^{-2}$	2.59321663 $10^{-2}$	2.04250289 $10^{-1}$	5.55384870 $10^{-2}$
6	-6.15230377 $10^{-3}$	-3.94194796 $10^{-3}$	-1.25846811 $10^{-1}$	-2.89978905 $10^{-2}$	-5.88972872 $10^{-1}$	-5.65349137 $10^{-2}$
8	2.69069927 $10^{-3}$	1.92550252 $10^{-3}$	1.94026824 $10^{-1}$	3.56078818 $10^{-2}$	1.78779922 $10^{-1}$	-3.46409964 $10^{-2}$
$\chi_c$						
0	4.73182256 $10^{-1}$	3.60327615 $10^{-1}$	4.73182256 $10^{-1}$	3.60327615 $10^{-1}$	4.73182256 $10^{-1}$	3.60327615 $10^{-1}$
2	-2.14752162 $10^{-1}$	-1.24947446 $10^{-1}$	-4.29504323 $10^{-1}$	-2.49894893 $10^{-1}$	-6.44256485 $10^{-1}$	-3.74842339 $10^{-1}$
4	9.57436401 $10^{-2}$	6.51283684 $10^{-2}$	5.88984198 $10^{-1}$	2.45225449 $10^{-1}$	1.47972167	5.40291243 $10^{-1}$
6	-3.93249095 $10^{-2}$	-3.25845479 $10^{-2}$	-8.44234559 $10^{-1}$	-2.81650591 $10^{-1}$	-4.00301487	-7.06439879 $10^{-1}$
8	1.51554530 $10^{-2}$	1.49996060 $10^{-2}$	1.22035314	3.56665468 $10^{-1}$	1.16033653 $10^{-1}$	5.01750366 $10^{-1}$